



HAL
open science

Population balance modelling of a continuous static mixer-based emulsification process

Noureddine Lebaz, Nida Sheibat-Othman

► **To cite this version:**

Noureddine Lebaz, Nida Sheibat-Othman. Population balance modelling of a continuous static mixer-based emulsification process. *Chemical Engineering Research and Design*, 2022, 7th International Conference on Population Balance Modelling 2022, 188, pp.645-654. 10.1016/j.cherd.2022.10.022 . hal-03815945

HAL Id: hal-03815945

<https://hal.science/hal-03815945v1>

Submitted on 27 Sep 2023

HAL is a multi-disciplinary open access archive for the deposit and dissemination of scientific research documents, whether they are published or not. The documents may come from teaching and research institutions in France or abroad, or from public or private research centers.

L'archive ouverte pluridisciplinaire **HAL**, est destinée au dépôt et à la diffusion de documents scientifiques de niveau recherche, publiés ou non, émanant des établissements d'enseignement et de recherche français ou étrangers, des laboratoires publics ou privés.

Population balance modelling of a continuous static mixer-based emulsification process

Noureddine Lebaz¹; Nida Sheibat-Othman^{1*}

¹ University of Lyon, Université Claude Bernard Lyon 1, CNRS, LAGEPP UMR 5007, F-69100, Villeurbanne, France

1 Abstract

Emulsions preparation using static mixers is investigated in this work. First, it is demonstrated that a fully continuous emulsification process is experimentally feasible through the direct pumping of the two immiscible phases separately into a set of static mixers. This process is advantageous, especially in the case of highly viscous fluids, compared to that employing a pre-emulsification step in stirred tanks which creates inhomogeneity in the sample in terms of the droplet size. Second, a population balance model is employed for the prediction of the droplet size distribution at the process outlet. To do so, a recently modified breakage kernel of Coualoglou and Tavlarides, accounting for droplet breakage within the inertial and dissipation subranges of isotropic turbulence, is used. In this work, we propose to calculate the second-order longitudinal structure function using semi-empirical formulas. Moreover, the kernel considers the droplet cohesive force due to the viscosity of the dispersed. While this term is sometimes neglected in the literature, we found that this is certainly due to the use of a limited range of variation of the dispersed phase viscosity for parameter identification. The developed model is validated against a large range of experimental data and showed very good prediction capabilities.

Keywords: Emulsification, static mixers, droplet breakage, turbulence, population balance.

* Corresponding author. Address : LAGEPP, Université Claude Bernard Lyon 1, bât 308G ESCPE-Lyon, 43 bd du 11 Novembre 1918, Villeurbanne 69622 France. Tel.: +33 04 72 43 18 50; Fax: +33 04 72 43 16 99
Email address: nida.othman@univ-lyon1.fr (Nida Sheibat-Othman)

2 Introduction

Liqui-liquid turbulent dispersions are complex physical systems in which one fluid is dispersed in the form of small droplets in a second non-miscible fluid (McClements, 2015). To minimize coalescence and avoid phase separation, specific surfactants may be incorporated into the system to lower the surface tension and stabilize the dispersion. One of the main physical characteristics of emulsions is their droplet size distribution (DSD) which affects their properties such as their aspect, texture, rheology and stability. Therefore, efforts have been made for the DSD prediction through different modelling strategies.

Since decades, modelling turbulent droplet breakage is based on the classical Kolmogorov-Hinze framework (Hinze, 1955). The main hypothesis of this framework is that the droplets of diameter d are broken exclusively by the surrounding turbulent eddies of the same size, despite the wide spectrum of turbulence length scales, and the fragmentation is effective if the pressure fluctuations due to velocity gradients are higher than the surface tension stresses (Perlekar et al., 2012; Yi et al., 2021). From the Kolmogorov-Hinze assumption, one may consider that the sub-droplet scale eddies have a negligible contribution on the droplet fragmentation process. For a long time, as turbulent eddies of different length scales are present simultaneously, it was experimentally difficult to disentangle them cleanly in order to assess their contribution when droplet breakage occurs (Cardesa et al., 2017). Very recently, (Qi et al., 2022) reported that, in the case of bubbles, instead of being elongated slowly and persistently by eddies at their own scales, they are fragmented by small eddies via a burst of intense local deformation within a short time. This affirmation was made possible thanks to experimental observations using a specific set-up in which eddies of different sizes are generated in a controlled manner. These experimental findings have been already predicted by direct numerical simulations (DNS) of emulsions in homogeneous isotropic turbulence where fluid properties are varied (e.g. dispersed phase volume fraction, viscosity ratio between the dispersed and continuous phases) (Crialesi-Esposito et al., 2022b, 2022a; Mukherjee et al., 2019; Rosti et al., 2019).

Population balance modelling of the time evolution of the DSD with regard to the physical chemistry and operating conditions prevailing in the system is now a well-established framework (Alopaeus et al., 1999; Becker et al., 2011). It allows the consideration of the different phenomena taking place at the droplet scale through sub-models such as breakage, coalescence and Ostwald ripening. By integration, the behavior of the dispersed phase at the process scale is then captured. In systems where non-homogeneous turbulence prevails (e.g.

stirred tanks, extraction columns), population balance models (PBM) are generally coupled with computational fluid dynamics (CFD) (Gao et al., 2016; Yu et al., 2020). The predictability of PBM is highly dependent on the reliability of the sub-models, referred to as kernels, used to describe the phenomena involved in the considered process. Different kernels are proposed in literature and reviewed by (Liao and Lucas, 2009) in the case of droplet breakage. Their derivation is generally based on the statistical theory of turbulence assuming that droplet breakage occurs exclusively in the inertial subrange of isotropic turbulence, i.e. the droplet breakage is mainly the consequence of inertia forces due to the interaction of vortices and droplets (Alopaeus et al., 1999; Coualoglou and Tavlarides, 1977; Luo and Svendsen, 1996; Ramkrishna, 1974). This results in the use of the Kolmogorov turbulence energy spectrum model. However, as discussed earlier, the assumption of droplet breakage by eddies whose sizes are exclusively within the inertial subrange of isotropic turbulence is not valid. Therefore, in the case of droplets whose diameters are outside the inertial subrange, the classical kernels are unable to provide reasonable predictions of the breakage rate (Karimi and Andersson, 2019). This is particularly the case for high viscosity emulsions (Hert and Rodgers, 2019). To overcome this issue, in the recent years, a limited number of studies proposed the extension of the kernels to the entire spectrum of isotropic turbulence (Castellano et al., 2019; Han et al., 2014; Karimi and Andersson, 2018; Solsvik and Jakobsen, 2016a, 2016b). These extensions were generally validated against experimental data available in literature, mainly liquid-liquid emulsification in stirred tanks (Han et al., 2014; Karimi and Andersson, 2019). It is worth noticing that this new framework requires the knowledge of the turbulent kinetic energy and the energy dissipation rate in the system locally, which may be obtained through CFD simulations. So, CFD-PBM coupling would be required to tackle the spatial heterogeneity of these quantities in stirred tanks for instance (Castellano et al., 2019).

Recently, we investigated droplet breakage in a semi-continuous emulsification process using static mixers experimentally and numerically within the framework of the entire spectrum of turbulent energy (Lebaz et al., 2022). For this, coarse pre-emulsions were prepared in a stirred tank and pumped through static mixers for further breakage (Lebaz and Sheibat-Othman, 2019a). A numerical study on the flow field (CFD) inside the mixers showed that they present a very good dispersive behavior with almost spatially homogeneous characteristics (Azizi et al., 2022). It was also shown that droplet breakage occurs within the inertial and dissipative subranges of turbulence, while the energy containing subrange has a negligible contribution.

Due to these findings, (Lebaz et al., 2022) extended the breakage kernel to the dissipative subrange of turbulence by using the mean energy dissipation rate as input.

In this work, turbulent liquid-liquid emulsification in a fully continuous process using SMX+ type static mixers is investigated (without pre-emulsification in a stirred tank) and compared to the semi-continuous process (with pre-emulsification in a stirred tank) presented in (Lebaz et al., 2022). Moreover, a PBM accounting for droplet breakage occurring within the inertial and dissipation subranges of turbulence is proposed and validated against experimental data. The breakage kernel computation is based on the use of the semi-empirical formula proposed by Kolmogorov for the inertial subrange and Sawford and Hunt for the dissipation subrange of turbulence (Kolmogorov, 1941; Sawford and Hunt, 1986). This is shown to be a very good alternative instead of solving numerically non-linear constraints as in (Lebaz et al., 2022). Finally, the experiments realized in the new set-up allowed for a better identification of the kernel parameters, as the difference between the inlet and the outlet DSD is bigger and a wider range of variation of the operating conditions is considered.

3 Materials and experimental methods

3.1 Emulsion ingredients

The different direct oil-in-water emulsions are prepared first by mixing ultrapure water (Synergy unit system, Millipore, France), glycerol (VWR Chemicals, France) as continuous phase viscosity enhancer, and Polysorbate 20 (Tween[®]20, Sigma-Aldrich, Germany) as surfactant (~2 g/L). The dispersed phase is constituted of silicone oil (Sigma-Aldrich, Germany) of different viscosities.

3.2 Experimental set-ups

Two different emulsification set-ups have been used in this study. In the first one (Figure 1), a pre-emulsion is prepared in a stirred tank by mixing the two immiscible phases prior to its injection through a set of 20 SMX+ elements (Lebaz and Sheibat-Othman, 2019a). The different pre-emulsions are prepared in the same conditions of mixing at 500 rpm for 2 hours using a Rushton turbine in a 1 L baffled tank. In the second set-up (Figure 2), the two phases are pumped separately through a first set of 10 mixing elements for pre-mixing followed by a second set of 10 SMX+ mixers. MCP-Z Ismatec gear pumps are used in the two set-ups for pumping the pre-emulsion (first set-up) and the two phases individually (second set-up). In the second set-up, as the flow rate of the dispersed phase is 100 times lower than that of the

continuous phase, a Y-junction is used by ensuring that the oil smaller tube is injected into the bigger tube of the continuous phase, which was found to enhance the stability of both flow rates.

The pressure drop induced by the presence of the mixers is measured by a pressure gauge (Keller LEO1: 0-3 bar, ± 3 mbar, Germany) placed at the upstream of the static mixers. To assess the efficiency of the static mixers in breaking the dispersed phase droplets, two samples are withdrawn systematically at the inlet and the outlet of the mixers for the first set-up and at the inlet and the outlet of the second set of static mixers for the second set-up. The DSD of these samples is measured offline using a laser diffraction particle size analyzer (Mastersizer 3000, Malvern Instruments, France), after important dilution in pure water, and the measurement is repeated three times for each sample. The Sulzer SMX+ static mixers are porous cylinders having the same height and diameter of 5 mm with a specific surface area of $1527 \text{ m}^2 \cdot \text{m}^{-3}$, a global porosity of 75% and a hydraulic diameter of 1.42 mm (Lebaz and Sheibat-Othman, 2019b).

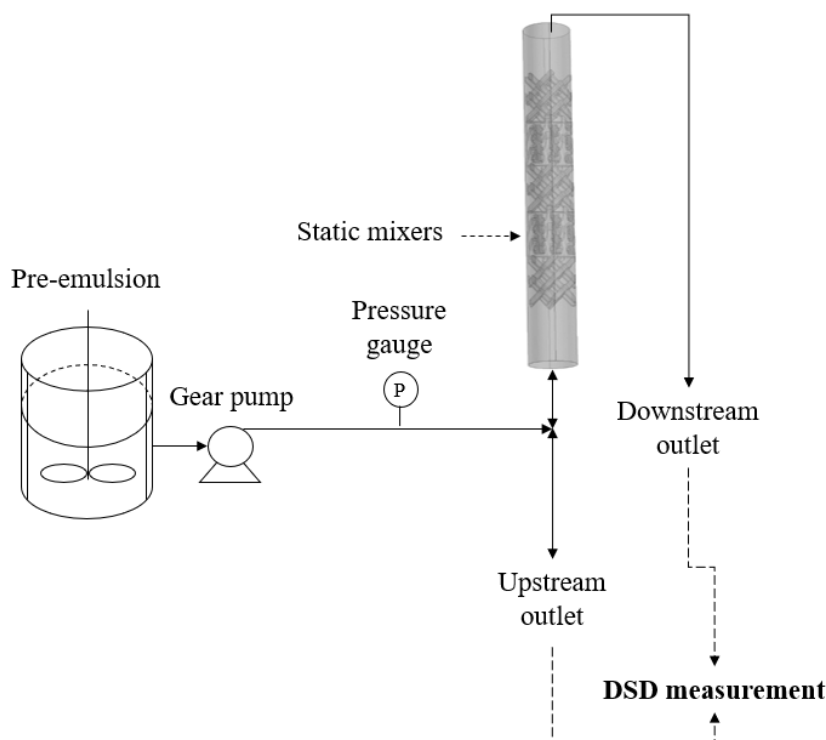


Figure 1: First experimental set-up with a pre-emulsion using a stirred tank followed by emulsification through SMX+ static mixers.

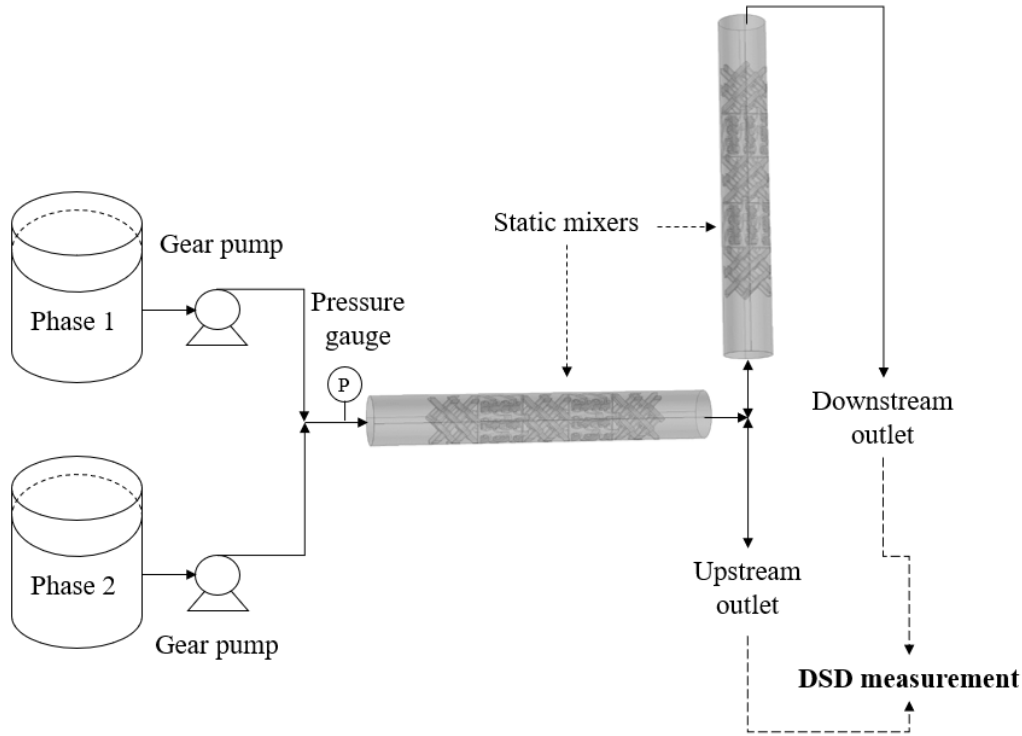


Figure 2: Second experimental set-up with a pre-emulsion using a first set of 10 SMX+ static mixers followed by emulsification through a second set of 10 SMX+ static mixers.

The set of experiments carried out using the second set-up (Figure 2) are summarized in Table 1, while those achieved using the first set-up (Figure 1) is reported in our previous work (Lebaz et al., 2022) .

Table 1: List of experiments carried out by varying the viscosity of the continuous/dispersed phases and the Reynolds number using the set-up 2 (Figure 2)

Exp. n°	Water (wt %)	Glycerol (wt %)	μ_c [mPa.s]	μ_d [mPa.s]	Re_h	ε [m ² .s ⁻³]
1	100	0	1	10	1000	224
2	54.3	45.7	5	10	300	484
3	42.2	57.8	10	10	300	2928
4	100	0	1	20	1000	224
5	54.3	45.7	5	20	300	484
6	42.2	57.8	10	20	300	2927

7	100	0	1	50	1000	224
8	54.3	45.7	5	50	300	484
9	42.2	57.8	10	50	300	2927
10	100	0	1	100	1000	224
11	54.3	45.7	5	100	300	484
12	42.2	57.8	10	100	300	2927
13	100	0	1	200	1000	224
14	54.3	45.7	5	200	300	484
15	42.2	57.8	10	200	300	2927
16	100	0	1	350	1000	224
17	54.3	45.7	5	350	300	484
18	42.2	57.8	10	350	300	2927

The hydraulic Reynolds number is estimated as:

$$Re_h = \frac{\rho_c u_s D_h}{\varphi \mu_c} \quad (1)$$

Where u_s is the superficial velocity, φ is the porosity of the mixers, D_h is the mixer's hydraulic diameter, and ρ_c and μ_c are the apparent density and viscosity of the continuous phase, respectively (Chabanon et al., 2017). As reported by (Theron and Le Sauze, 2011), for turbulent emulsification, Re_h should be higher than 260, which is the case for all the experiments reported in Table 1.

4 Numerical aspects

As reported in (Lebaz et al., 2022), during emulsification using SMX+ static mixers, droplet breakage occurs within the inertial and dissipation subranges of turbulence. Hence, the PBM of this process should incorporate this information in the breakage kernel instead of using the classical kernels based on the Kolmogorov's energy spectrum valid only for the inertial subrange of turbulence. To do so, it was previously suggested to use the Pope's energy spectrum, which introduces a nondimensional function f_η accounting for the dissipation part of

the spectrum (equation 3 in Table 2) (Lebaz et al., 2022). The transition between the two subranges occurs at a length scale of 15η , where η is the Kolmogorov length scale defined in equation 4. The introduction of the truncated Pope's energy spectrum requires the determination of the parameter c_η through the constraint given by equation 5. Similarly, a constraint is defined for the energy-containing subrange of turbulence, but we found that it converges to one in our case (Lebaz et al., 2022). So, the energy spectrum is reduced to the inertial and dissipation subranges, and the problem requires the estimation of only the dissipation-range function f_η , which was achieved by solving numerically the constraint (equation 5), allowing the identification of the parameter c_η .

As the mean turbulent fluctuating velocity of the vortices is responsible for the droplet deformation and breakage, the energy conveyed by these eddies may be approximated by the second-order longitudinal structure function $\langle[\delta u]^2\rangle$ which may be computed through the formula of Davidson in equation 8 (Davidson, 2015). In the present work, we will use the approximation of the second-order longitudinal structure function through the combination of the semi-empirical formulas proposed by Kolmogorov for the inertial subrange (Kolmogorov, 1941) and by Sawford and Hunt for the dissipation subrange (Sawford and Hunt, 1986) given in equation 9, instead of equation 8 (so equations 2, 3, 5 and 8 are not used in the new model). These semi-empirical formulas allows to accelerate the computation and avoid convergence errors that may occur during optimization (done to solve the constraint in equation 5 numerically in our previous work (Lebaz et al., 2022)).

The phenomenological Coualoglou and Tavlarides model framework is adopted for the formulation of the droplet breakage kernel (Coualoglou and Tavlarides, 1977). As pointed out in (Lebaz et al., 2022), two main modifications are brought to this kernel: i) the breakage criterion considers the cohesive forces of the dispersed entities due to the surface tension as well the internal viscosity, which act against the disruptive eddies; ii) the kernel is reformulated in order to be valid for both inertial and dissipation subranges of isotropic turbulence. The only difference here is the proposition of a simplified formula of $\langle[\delta u]^2\rangle(\lambda)$.

Regarding the daughter size distribution, a beta function is adopted (equation 13). This function assumes that breakage event produces most likely symmetric daughters (Li et al., 2017). Other daughter size distribution forms were tested and similar results as those of the beta function were obtained. The breakage kernel and the daughter size distribution are sub-models of the population balance equation (PBE) given in equation 11. The PBE in this case considers only

the droplet breakage since coalescence and Ostwald ripening are negligible. Moreover, as the flow field characteristics in the process are almost spatially uniform, the time evolution of the DSD is the target output of the PBE-based model and the mean energy dissipation rate is accessible experimentally through the measurement of the pressure drop (equation 6). The homogeneous PBE is integrated over a time span given by the residence time in the static mixer element series.

Table 2: Summary of the energy spectrum model and population balance equations

Turbulence spectrum of Pope for the inertial and dissipative subranges (Pope, 2001)	$E(\kappa) = C \varepsilon^{\frac{2}{3}} \kappa^{-\frac{5}{3}} f_{\eta}(\kappa\eta)$	(2)
Dissipation subrange (Pope, 2001)	$f_{\eta}(\kappa\eta) = \exp\left\{-\beta\left([\kappa\eta]^4 + c_{\eta}^4\right)^{1/4} - c_{\eta}\right\}$	(3)
Kolmogorov length scale (Kolmogorov, 1941)	$\eta = \left(\frac{\nu^3}{\varepsilon}\right)^{1/4}$	(4)
Constraint (Pope, 2001)	$\varepsilon = \int_0^{\infty} 2\nu\kappa^2 E(\kappa) d\kappa$	(5)
Volume-average turbulent energy dissipation rate	$\bar{\varepsilon} = \frac{\Delta P u_i}{\rho c L_s}$	(6)
Interstitial velocity within the mixers	$u_i = \frac{u_s}{\varphi} = \frac{4Q}{\pi D_s^2} \frac{1}{\varphi}$	(7)
Second-order longitudinal structure function (Davidson, 2015)	$\langle[\delta u]^2\rangle(\lambda) = \frac{4}{3} \int_0^{\infty} E(\kappa) \left[1 + 3 \left\{\frac{\cos(\kappa\lambda)}{(\kappa\lambda)^2} - \frac{\sin(\kappa\lambda)}{(\kappa\lambda)^3}\right\}\right] d\kappa$	(8)
Semi-empirical formula for the second-order longitudinal structure function (Kolmogorov, 1941; Sawford and Hunt, 1986)	$\langle[\delta u]^2\rangle(\lambda) = C(\varepsilon\lambda)^{2/3} \left(\frac{\lambda^2}{\lambda_d^2 + \lambda^2}\right)^{2/3}$	(9)
Length scale relation (Sawford and Hunt, 1986)	$\lambda_d = (15C)^{3/4} \eta$	(10)
Population balance equation (Narsimhan et al., 1979)	$\frac{\partial n(v,t)}{\partial t} = \int_v^{\infty} b(v,v')g(v')n(v',t)dv' - g(v)n(v,t)$	(11)

Breakage kernel (Lebaz et al., 2022)	$g(d) = \frac{c_1 \sqrt{u^2(d)}}{d} \exp\left(-\frac{c_2 \sigma}{\rho_d d \sqrt{u^2(d)}} - \frac{c_3 \mu_d}{\rho_d^{3/2} \rho_c^{-1/2} d \sqrt{u^2(d)}}\right)$	(12)
Breakage daughter size distribution (Hsia and Tavlarides, 1983)	$b(v, v') = \frac{60}{v'} \left(\frac{v}{v'}\right)^2 \left(1 - \frac{v}{v'}\right)^2$	(13)

The numerical integration of the PBE was achieved using the finite-volume method of (Kumar et al., 2009). Details on the PBE integration methodology may be found in (Lebaz and Sheibat-Othman, 2019a). Finally, the breakage kernel parameters (C_1 , C_2 and C_3 in equation 12) were identified through an absolute difference minimization procedure between all the experimental DSD in volume and the corresponding numerical predictions. The least-square non-linear solver *lsqnonlin* (Matlab) with a *Multistart* option was used for this purpose. As will be shown hereafter, the wide range of variation of the viscosity of the oil phase was necessary in order to better identify the parameter C_3 , which would be found to be negligible otherwise.

5 Results and discussion

5.1 Comparison of emulsification procedures

As two different emulsification procedures have been investigated, a comparison between the emulsification results in both cases is first presented. Figure 3 shows the evolution of the DSD between the inlet and the outlet of the process for various viscosities of the continuous and the dispersed phases.

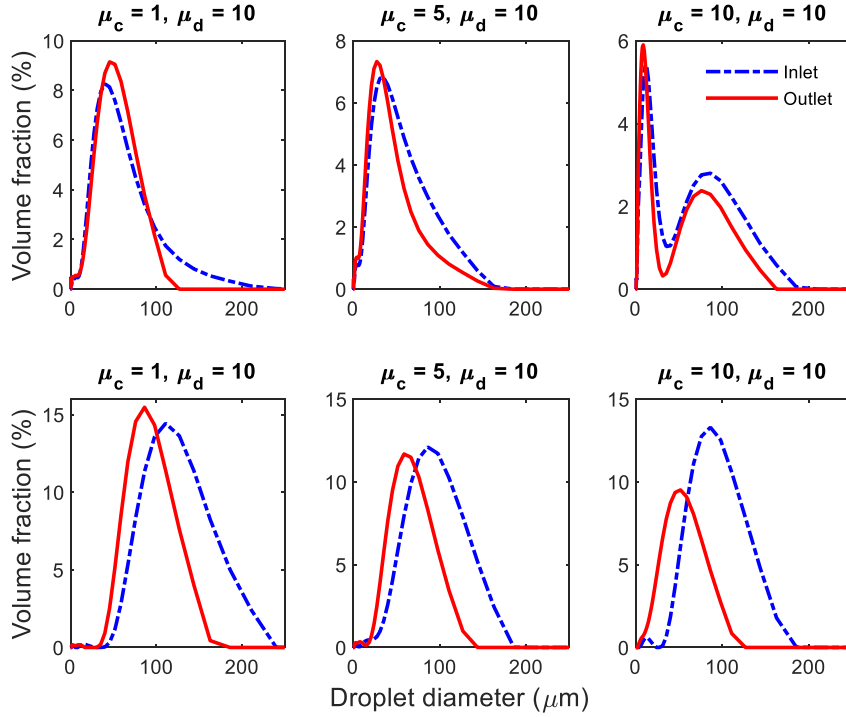


Figure 3: Inlet and outlet DSD as a function of the droplet diameter, for different viscosities (in mPa.s) of the continuous phase. The three subplots on the top refer to the first experimental set-up while the three subplots on the bottom are obtained with the second experimental set-up (experiments n° 1, 3 and 4 in Table 1).

As can be seen in Figure 3, from the first set-up (3 subplots on the top of the figure), when the viscosity of the continuous phase increases and gets close to the dispersed phase viscosity, the DSD tends progressively towards a bimodal distribution. This is the case originally for the inlet DSDs (pre-emulsions) which are generated in the stirred tank. Indeed, as the viscosity of the continuous phase increases, the energy dissipation rate in the stirred tank becomes concentrated around the impeller while it vanishes rapidly when moving away from the mechanical stirrer towards the tank walls. Also, the mixing efficiency decreases as the flow velocity decreases, which reduces the motion of droplets within the different parts of the reactor. As a result, only part of the droplets would be exposed to the high energy dissipated by the impeller. This is responsible of the persistence of droplets with high size (second mode of the DSD) even at high mixing times (2 hours in our case). For all viscosities, the outlet DSD shifts towards smaller sizes after passing within the static mixers, which demonstrates their efficiency, but the initial global shape remains unchanged, whether monomodal or bimodal. So, in this set-up, the bimodal DSD shape is mainly caused by the pre-emulsification step, and not to a different

breakage mechanism like for instance evolving to a U-shape daughter size distribution when increasing the viscosity ratio of the continuous phase to the dispersed phase.

In the case of a pre-emulsification carried out using SMX+ static mixers (3 subplots on the bottom of the figure, obtained using the second experimental set-up), even at high continuous phase viscosity, the inlet DSD remains monomodal. This demonstrates the very good efficiency of the SMX+ static mixers to break the oil droplets in a continuous way with a pressure drop less than 1 bar and a residence time of less than 0.1 second in all cases. The uniformity of the DSD obtained through the SMX+ mixers is due to the spatial uniformity of the energy dissipation rate thanks to the homogeneity of the fluid flow patterns in this confined system unlike in stirred tanks (Azizi et al., 2022). At the outlet of the system, a noticeable DSD shift towards the small sizes is pointed out. The global shape of the distributions remains almost similar to that of the inlet, but the addition of SMX+ elements induces further droplet breakage.

Besides the effect of the continuous phase viscosity on the uniformity of mixing, it has an effect on the size of droplets. For the same Reynolds (experiments 2 and 3 in Table 1), smaller droplets are obtained when increasing the viscosity of the continuous phase. Note that a higher flow rate is required to ensure the same Reynolds in this case, which increases the energy dissipation rate. It is easier to affirm this hypothesis in the second set-up as we have a monomodal distribution. The effect of the dispersed phase viscosity will be discussed later while comparing to the model.

This rapid and qualitative comparison between the two experimental set-ups demonstrates that a fully continuous emulsification process is practically feasible through the use of static mixers. Moreover, this system shows a remarkable efficiency with a compact design, reduced energy consumption and a very low residence time (high productivity). The following discussion will be dedicated exclusively to the results obtained using the second experimental set-up, as it better describes the phenomena occurring under variable conditions, and should allow for a better identification of the kernel and its parameters.

5.2 Validation of the second-order longitudinal structure function

In our previous work, the second-order longitudinal structure function proposed by (Davidson, 2015) was employed (equation 8). Its numerical computation was achieved in two parts: i) the adjustable parameter c_η was determined through the numerical solution of the non-linear constraint in equation 5 using the Matlab function *fsolve*; ii) the integral within equation 8 was computed using the function *ode45* which is a non-stiff differential equation solver employed

for its numerical stability. As discussed by (Solsvik and Jakobsen, 2016b), these computations are time-consuming. To overcome this issue, the semi-empirical model proposed both by Kolmogorov (inertial subrange) and by Sawford and Hunt (dissipation subrange) is preferred here (Kolmogorov, 1941; Sawford and Hunt, 1986). A comparison of the predictions of the two models is shown in Figure 4.

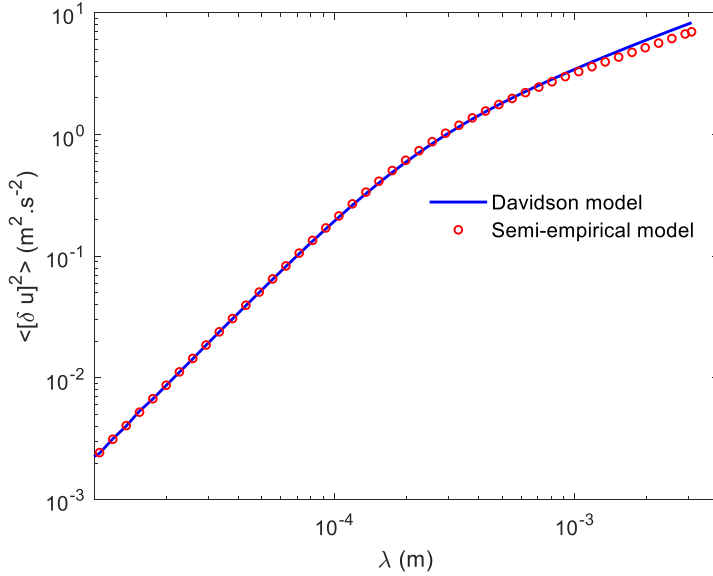


Figure 4: Comparison of the second-order longitudinal structure function obtained through the model of Davidson (equation 8) and using the semi-empirical model (equation 9). The data reported here is for the experiment n° 4 in Table 1.

As shown in Figure 4, the two different models provide the same predictions for the second-order structure function. The model of Davidson requires the use of a non-linear solver coupled to a numerical integrator, resulting in a high computational cost unlike the semi-empirical model. Hence, when the energy spectrum is reduced to the inertial and dissipation subranges of turbulence, the semi-empirical model is advantageous. It will be then employed in this study. It is worth noticing that even for the full energy spectrum, semi-empirical models are available in literature (Solsvik, 2017; Solsvik and Jakobsen, 2016b).

5.3 Numerical predictions

As explained before, a global optimization procedure was carried out using all the experiments of Table 1 for the identification of the model parameters. The numerical values of the three parameters are given in Table 3.

Table 3: Identified breakage kernel parameters using all the available experimental data

C_1	C_2	C_3
-------	-------	-------

5.3×10^{-3}	2.5×10^{-2}	1.6×10^{-1}
----------------------	----------------------	----------------------

5.3.1 Effect of the dispersed phase viscosity

The viscosity of the dispersed phase (silicone oil) was varied from 10 to 350 mPa.s. To illustrate the effect of this parameter on the DSD, the experimental and the numerical results are compared in Figure 5 in the case of $\mu_c=5$ mPa.s.

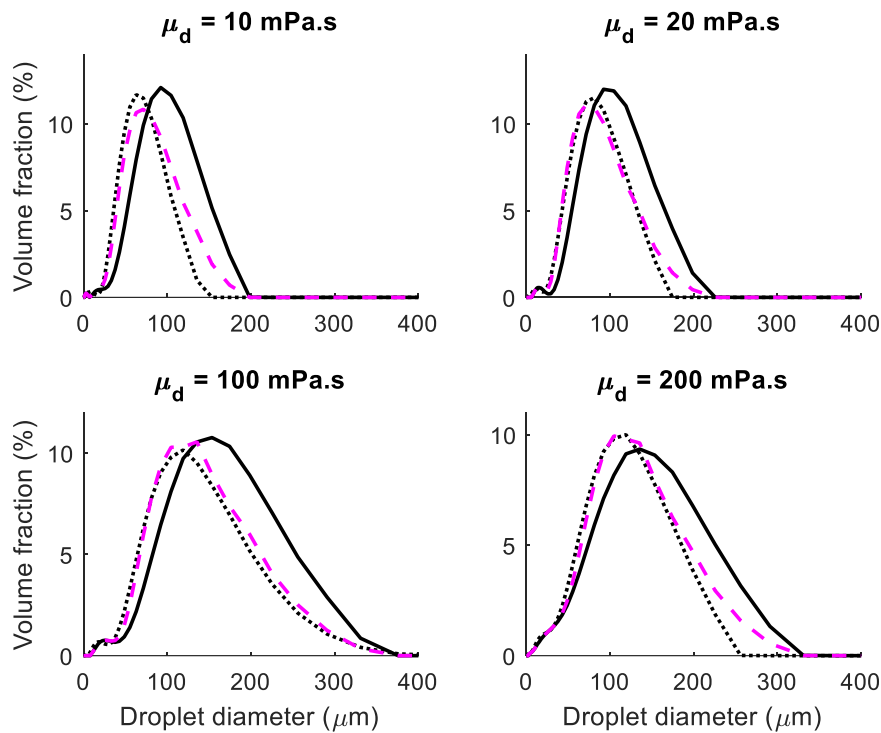


Figure 5: Effect of the dispersed phase viscosity on the DSD at $\mu_c=5$ mPa.s: comparison between the experimental results and PBM predictions. The continuous black line refers to the inlet DSD, the dotted black line is the experimental outlet DSD and the dashed magenta line is the numerical outlet DSD.

From Figure 5, as the dispersed phase viscosity increases (at constant hydraulic Reynolds of 300 and continuous phase viscosity of 5 mPa.s), the DSD at the outlet of the first static mixer series (pre-emulsion) shifts towards bigger diameters. This is due to the enhanced cohesion of the oil droplets which become more difficult to break. Moreover, the DSD difference between the inlet and the outlet of the mixers is reduced since the breakage efficiency decreases when the viscosity of the oil increases. Note that the different experiments shown in Figure 5 are carried out at the same Re_h .

Regarding the numerical predictions of the developed PBM, they remain very good for the different oil viscosities since the breakage frequency expression accounts for the contribution

of the dispersed phase viscosity to the cohesion of the oil droplets. It is worth noticing that the value of the parameter C_3 is not negligible compared to the two other parameters which means that the model is sensitive to the dispersed phase viscosity. The good identification is due to the wide range variation of the dispersed phase viscosity, used for identification, unlike in (Lebaz et al., 2022).

5.3.2 Effect of the continuous phase viscosity

The viscosity of the continuous phase was varied from 1 to 10 mPa.s and the hydraulic Reynolds number was kept constant (around 300) for the higher viscosities (5 and 10 mPa.s). At the lowest viscosity ($\mu_c=1$ mPa.s), the hydraulic Reynolds number was around 1000 since at $Re_h=300$, the change in the DSD between the input and the output was not experimentally measurable for this particular case. The effect of the continuous phase viscosity on the DSD is shown in Figure 6 for two different oil viscosities ($\mu_d=20$ mPa.s and $\mu_d=100$ mPa.s).

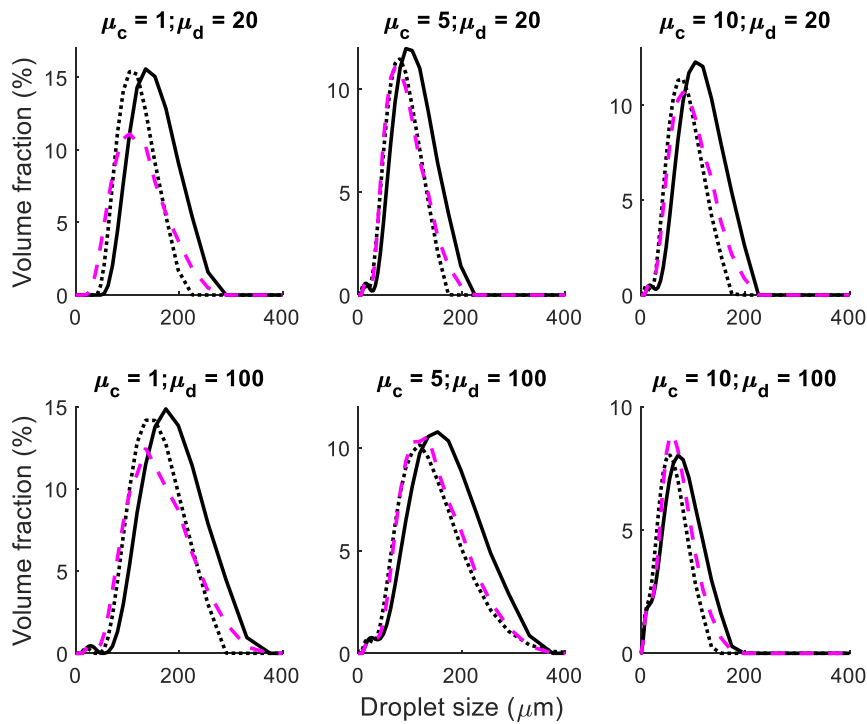


Figure 6: Effect of the continuous phase viscosity on the DSD at $\mu_d=20$ mPa.s and $\mu_d=100$ mPa.s: comparison between the experimental results and the PBM predictions. The continuous black line refers to the inlet DSD, the dotted black line is the experimental outlet DSD and the dashed magenta line is the numerical outlet DSD. All the viscosities are in mPa.s.

As reported before, even at high continuous phase viscosity, the DSD formed thanks to the mixing properties of the SMX+ static mixers remain monomodal. To keep the Re_h constant (typically for $\mu_c=5$ and $\mu_c=10$ mPa.s), the flow rate is increased to compensate the viscosity

enhancement, leading to a higher energy dissipation rate, and so to a more efficient droplet breakage. This can be clearly seen for the inlets DSD of $\mu_c=5$ mPa.s and $\mu_d=100$ mPa.s which present a volume-based mean droplet size (d_{43}) of around 134 μm while the inlet DSD for $\mu_c=10$ mPa.s with the same oil viscosity has a d_{43} of about 55 μm . The predictions of the developed PBM remain very good whatever the viscosity of the continuous phase.

5.3.3 Overall predictions

To present the numerical results for all the experiments in Table 1 in a concise manner, the predicted volume-based mean droplet diameters of all the DSDs are compared to those obtained experimentally. The results are shown in Figure 7.

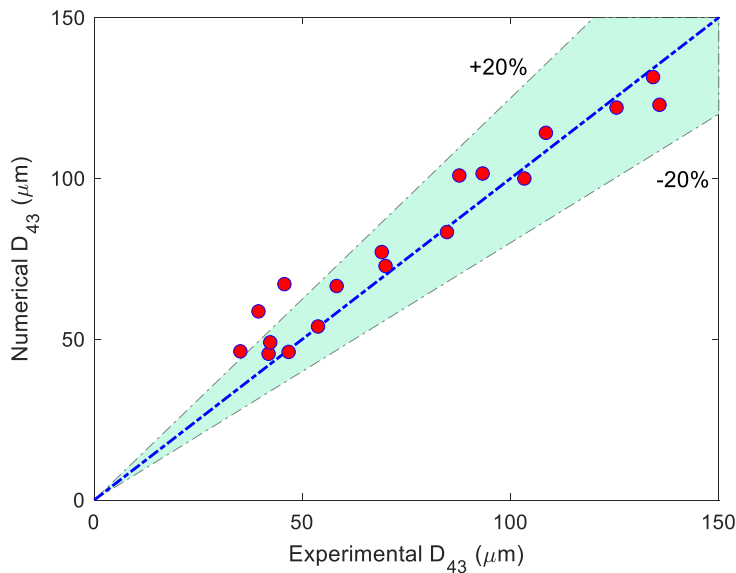


Figure 7: Comparison of the volume-based mean diameters (d_{43}) at the outlet of the system obtained in different conditions: PBM-based predictions vs experimental results

As shown in Figure 7, almost all the numerical predictions fall within the confidence interval of $\pm 20\%$. The volume-based mean diameter, which is one of the most frequently used properties of the DSD, is well predicted despite the wide interval of variation of the experimental parameters investigated in this study (flow rate, viscosity of the dispersed phase and that of the continuous phase). This demonstrates the reliability of the developed PBM based on the modification of the breakage frequency to consider both inertial and dissipation subranges of isotropic turbulence. It is worth noticing that, unlike all the available literature, where the extension of the kernels to the full turbulence spectrum requires CFD calculations, in our case, the turbulent energy dissipation rate, estimated through the measurement of the pressure drop in the system, was sufficient. Moreover, no optimization was required to compute

the spectrum parameters, which were calculated by analytical approximations. This is a noticeable difference which makes the use of the modified kernel straightforward.

6 Conclusions

In this study, turbulent emulsification using static mixers was investigated experimentally and numerically. First, it was shown experimentally that a complete continuous emulsification process using SMX+ static mixers was feasible by the direct pumping of the two immiscible phases through a set of mixing elements. It was demonstrated that even at high continuous phase viscosities, the process remains efficient and produces uniform DSDs unlike emulsification in stirred tanks which leads to bimodal distributions because of the spatially non-uniform energy dissipation rate distribution. While this non-uniformity of the quality of mixing in stirred tanks is clearly visible at high continuous phase viscosities, it is always present. Therefore, relying on experimental data realized totally or partially in stirred tanks may lead to a wrong interpretation of the phenomena and model identification, if not correctly coupled with spatial modelling and simulation (CFD).

A population balance model was proposed to describe droplet breakage inside the static mixers considering the contribution of eddies within both the inertial and dissipation ranges of isotropic turbulence. The disruptive force of these eddies acts against the droplet cohesive forces due to surface tension and viscosity of the dispersed phase. As a model input, only the mean energy dissipation rate is required in our case, and is estimated through the measurement of pressure drop. Moreover, for the sake of simplicity and numerical efficiency, the second-order longitudinal structure function in the breakage kernel was computed through a semi-empirical formula. After a global optimization procedure, the numerical outlet DSDs are compared to those obtained experimentally in different conditions. The good identification of parameters necessitates the inclusion of a wide variation of the operating conditions in the identification set, such as the viscosity of the dispersed phase. The developed model showed its ability to predict the outlet DSD with a good accuracy despite the wide range variation of the experimental conditions.

Unlike PBMs available in literature for emulsification processes, simplifications are made to allow the implementation of the model proposed in this study without the need for CFD simulations. The proposed model was demonstrated to be efficient and accurate under the different tested conditions and constitutes a step further for the use of sophisticated modelling strategies for industrial applications with a minimum computational cost.

7 Nomenclature

$b(v, v')$	Breakage daughter size distribution	m^{-3}
C	Kolmogorov constant (equation 1, $C = 1.62$)	-
C_i	Constants	-
c_η	Dissipative-scale constant of the Pope's model	-
d	Droplet diameter	m
D_H	Hydraulic diameter of the pipe	m
D_s	Diameter of the pipe	m
d_{43}	Volume-based mean droplet size	m
$E(\kappa)$	Energy spectrum	$\text{m}^3 \text{s}^{-2}$
f_η	Dissipative-scale function of the Pope's model	-
$g(v)$	Volume-based breakage frequency	s^{-1}
L_s	Length of the SMX+ mixer element	m
$n(v, t)$	Number-based density function	m^{-4}
ΔP	Pressure drop	Pa
Q	Volume flow rate	$\text{m}^3 \text{s}^{-1}$
t	Time	s
\bar{u}	Mean velocity in a turbulent eddy	m s^{-1}
u_i	Interstitial velocity	m s^{-1}
u_s	Superficial velocity	m s^{-1}
$\langle [\delta u]^2 \rangle$	One-dimensional second-order longitudinal structure function	$\text{m}^2 \text{s}^{-2}$
Re_h	Hydraulic Reynolds number	-
v, v'	Droplet volume	m^3

Greek letters

β	Constant (equation 3, $\beta = 5.2$)	-
ε	Energy dissipation rate	$\text{m}^2 \text{s}^{-3}$
$\bar{\varepsilon}$	Volume-average turbulent energy dissipation rate	$\text{m}^2 \text{s}^{-3}$
η	Kolmogorov length scale	m
κ	Wavenumber	m^{-1}
λ	Eddy size	m
λ_d	Length scale for the transition from the inertial to the dissipation subrange of turbulence	m
μ_c	Dynamic viscosity of the continuous phase	Pa s
μ_d	Dynamic viscosity of the dispersed phase	Pa s
ν	Kinematic viscosity of the continuous phase	$\text{m}^2 \text{s}^{-1}$
ρ_c	Continuous phase density	kg m^{-3}
ρ_d	Dispersed phase density	kg m^{-3}
σ	Surface tension	N m^{-1}
φ	Global porosity of the static mixers	-

8 References

- Alopaeus, V., Koskinen, J., Keskinen, K.I., 1999. Simulation of the population balances for liquid–liquid systems in a nonideal stirred tank. Part 1 Description and qualitative validation of the model. *Chemical Engineering Science* 54, 5887–5899.
- Azizi, F., Abou-Hweij, W., Lebaz, N., Sheibat-Othman, N., 2022. A numerical evaluation of flows through an SMX-Plus mixer. *Chemical Engineering Research and Design* 178, 382–394. <https://doi.org/10.1016/j.cherd.2021.12.030>
- Becker, P.J., Puel, F., Henry, R., Sheibat-Othman, N., 2011. Investigation of Discrete Population Balance Models and Breakage Kernels for Dilute Emulsification Systems. *Ind. Eng. Chem. Res.* 50, 11358–11374. <https://doi.org/10.1021/ie2006033>
- Cardesa, J.I., Vela-Martín, A., Jiménez, J., 2017. The turbulent cascade in five dimensions. *Science* 357, 782–784. <https://doi.org/10.1126/science.aan7933>
- Castellano, S., Carrillo, L., Sheibat-Othman, N., Marchisio, D., Buffo, A., Charton, S., 2019. Using the full turbulence spectrum for describing droplet coalescence and breakage in industrial liquid-liquid systems: Experiments and modeling. *Chemical Engineering Journal* 374, 1420–1432. <https://doi.org/10.1016/j.cej.2019.06.032>

- Chabanon, E., Sheibat-Othman, N., Mdere, O., Valour, J.P., Urbaniak, S., Puel, F., 2017. Drop size distribution monitoring of oil-in-water emulsions in SMX+ static mixers: Effect of operating and geometrical conditions. *International Journal of Multiphase Flow* 92, 61–69. <https://doi.org/10.1016/j.ijmultiphaseflow.2017.03.001>
- Coulaloglou, C.A., Tavlarides, L.L., 1977. Description of interaction processes in agitated liquid-liquid dispersions. *Chemical Engineering Science* 32, 1289–1297.
- Crialesi-Esposito, M., Chibbaro, S., Brandt, L., 2022a. The interaction of droplet dynamics and turbulence cascade. <https://doi.org/10.48550/arXiv.2206.08055>
- Crialesi-Esposito, M., Rosti, M.E., Chibbaro, S., Brandt, L., 2022b. Modulation of homogeneous and isotropic turbulence in emulsions. *Journal of Fluid Mechanics* 940. <https://doi.org/10.1017/jfm.2022.179>
- Davidson, P., 2015. *Turbulence: an introduction for scientists and engineers*. Oxford University Press.
- Gao, Z., Li, D., Buffo, A., Podgórska, W., Marchisio, D.L., 2016. Simulation of droplet breakage in turbulent liquid-liquid dispersions with CFD-PBM: Comparison of breakage kernels. *Chemical Engineering Science* 142, 277–288. <https://doi.org/10.1016/j.ces.2015.11.040>
- Han, L., Gong, S., Li, Y., Gao, N., Fu, J., Liu, Z., 2014. Influence of energy spectrum distribution on drop breakage in turbulent flows. *Chemical Engineering Science* 117, 55–70.
- Hert, S.C.D., Rodgers, T.L., 2019. On the steady-state drop size distribution in stirred vessels. Part II: Effect of continuous phase viscosity. *AIChE Journal* 65, e16556. <https://doi.org/10.1002/aic.16556>
- Hinze, J.O., 1955. Fundamentals of the hydrodynamic mechanism of splitting in dispersion processes. *AIChE Journal* 1, 289–295. <https://doi.org/10.1002/aic.690010303>
- Hsia, M.A., Tavlarides, L.L., 1983. Simulation analysis of drop breakage, coalescence and micromixing in liquid-liquid stirred tanks. *The Chemical Engineering Journal* 26, 189–199.
- Karimi, M., Andersson, R., 2019. Dual mechanism model for fluid particle breakup in the entire turbulent spectrum. *AIChE Journal* 65, e16600.
- Karimi, M., Andersson, R., 2018. An exploratory study on fluid particles breakup rate models for the entire spectrum of turbulent energy. *Chemical Engineering Science* 192, 850–863.
- Kolmogorov, A.N., 1941. Dissipation of energy in locally isotropic turbulence, in: *Dokl. Akad. Nauk SSSR*. pp. 16–18.
- Kumar, J., Warnecke, G., Peglow, M., Heinrich, S., 2009. Comparison of numerical methods for solving population balance equations incorporating aggregation and breakage. *Powder Technology* 189, 218–229.
- Lebaz, N., Azizi, F., Sheibat-Othman, N., 2022. Modeling Droplet Breakage in Continuous Emulsification Using Static Mixers in the Framework of the Entire Spectrum of Turbulent Energy. *Ind. Eng. Chem. Res.* 61, 541–553. <https://doi.org/10.1021/acs.iecr.1c03529>
- Lebaz, N., Sheibat-Othman, N., 2019a. A population balance model for the prediction of breakage of emulsion droplets in SMX+ static mixers. *Chemical Engineering Journal* 361, 625–634. <https://doi.org/10.1016/j.cej.2018.12.090>
- Lebaz, N., Sheibat-Othman, N., 2019b. Modeling Emulsification in Static Mixers: Equilibrium Correlations versus Population Balance Equations. *Chemical Engineering & Technology* 42, 1691–1701. <https://doi.org/10.1002/ceat.201900109>
- Li, D., Buffo, A., Podgórska, W., Marchisio, D.L., Gao, Z., 2017. Investigation of droplet breakup in liquid-liquid dispersions by CFD-PBM simulations: The influence of the

- surfactant type. *Chinese Journal of Chemical Engineering* 25, 1369–1380. <https://doi.org/10.1016/j.cjche.2017.01.014>
- Liao, Y., Lucas, D., 2009. A literature review of theoretical models for drop and bubble breakup in turbulent dispersions. *Chemical Engineering Science* 64, 3389–3406.
- Luo, H., Svendsen, H.F., 1996. Theoretical model for drop and bubble breakup in turbulent dispersions. *AIChE Journal* 42, 1225–1233. <https://doi.org/10.1002/aic.690420505>
- McClements, D.J., 2015. *Food emulsions: principles, practices, and techniques*. CRC press.
- Mukherjee, S., Safdari, A., Shardt, O., Kenjereš, S., Akker, H.E.A.V. den, 2019. Droplet–turbulence interactions and quasi-equilibrium dynamics in turbulent emulsions. *Journal of Fluid Mechanics* 878, 221–276. <https://doi.org/10.1017/jfm.2019.654>
- Narsimhan, G., Gupta, J.P., Ramkrishna, D., 1979. A model for transitional breakage probability of droplets in agitated lean liquid-liquid dispersions. *Chemical Engineering Science* 34, 257–265.
- Perlekar, P., Biferale, L., Sbragaglia, M., Srivastava, S., Toschi, F., 2012. Droplet size distribution in homogeneous isotropic turbulence. *Physics of Fluids* 24, 065101. <https://doi.org/10.1063/1.4719144>
- Pope, S.B., 2001. *Turbulent flows*. IOP Publishing.
- Qi, Y., Tan, S., Corbitt, N., Urbanik, C., Salibindla, A.K.R., Ni, R., 2022. Fragmentation in turbulence by small eddies. *Nat Commun* 13, 469. <https://doi.org/10.1038/s41467-022-28092-3>
- Ramkrishna, D., 1974. Drop-breakage in agitated liquid–liquid dispersions. *Chemical Engineering Science* 29, 987–992. [https://doi.org/10.1016/0009-2509\(74\)80090-4](https://doi.org/10.1016/0009-2509(74)80090-4)
- Rosti, M.E., Ge, Z., Jain, S.S., Dodd, M.S., Brandt, L., 2019. Droplets in homogeneous shear turbulence. *Journal of Fluid Mechanics* 876, 962–984. <https://doi.org/10.1017/jfm.2019.581>
- Sawford, B.L., Hunt, J.C.R., 1986. Effects of turbulence structure, molecular diffusion and source size on scalar fluctuations in homogeneous turbulence. *Journal of Fluid Mechanics* 165, 373–400. <https://doi.org/10.1017/S0022112086003142>
- Solsvik, J., 2017. Turbulence modeling in the wide energy spectrum: Explicit formulas for Reynolds number dependent energy spectrum parameters. *European Journal of Mechanics-B/Fluids* 61, 170–176.
- Solsvik, J., Jakobsen, H.A., 2016a. A review of the statistical turbulence theory required extending the population balance closure models to the entire spectrum of turbulence. *AIChE Journal* 62, 1795–1820.
- Solsvik, J., Jakobsen, H.A., 2016b. Development of fluid particle breakup and coalescence closure models for the complete energy spectrum of isotropic turbulence. *Industrial & Engineering Chemistry Research* 55, 1449–1460.
- Theron, F., Le Sauze, N., 2011. Comparison between three static mixers for emulsification in turbulent flow. *International Journal of Multiphase Flow* 37, 488–500.
- Yi, L., Toschi, F., Sun, C., 2021. Global and local statistics in turbulent emulsions. *Journal of Fluid Mechanics* 912. <https://doi.org/10.1017/jfm.2020.1118>
- Yu, X., Zhou, H., Jing, S., Lan, W., Li, S., 2020. Augmented CFD–PBM Simulation of Liquid–Liquid Two-Phase Flows in Liquid Extraction Columns with Wettable Internal Plates. *Ind. Eng. Chem. Res.* 59, 8436–8446. <https://doi.org/10.1021/acs.iecr.0c01476>